

# SURFACE FLOW AND STRAIN OF THE ICE SHEET MEASURED BY A TRIANGULATION CHAIN IN MIZUHO PLATEAU

Renji NARUSE

*The Institute of Low Temperature Science, Hokkaido University,  
Kita-ku, Sapporo 060*

**Abstract:** Surveys of a triangulation chain extending 250 km along the parallel of 72°S in Mizuho Plateau, East Antarctica, were carried out in 1969 and 1973–1974. Obtained from them were horizontal and vertical components of surface velocities of the ice sheet at 141 stations and also principal strains, maximum shear strains, dilatations, and rotations of the surface ice in 140 triangles of the chain.

Horizontal velocities of the ice sheet showed small values in the vicinity of the Yamato Mountains, and maximum values of more than 20 m/year in a region between 39°E and 40°E. Direction of the flow vector was approximately identical with that of the large-scale maximum slope of the ice surface, but the direction and magnitude of the principal strain showed influence by small-scale surface undulations. In general, the direction of the maximum extension of strain was rather close to that of the ice flow. Tensile strains were more common than compressive strains almost all over Mizuho Plateau.

The vertical component of ice velocity was directed downward, which is characteristic of the submergence flow, in the region from 39°E eastward. The amount of snow accumulation was not enough to compensate the deficit of ice mass caused by the submergence flow along the triangulation chain. The mass budget was negative in the zone of 2400–2600 m in elevation in the Shirase drainage.

## 1. Introduction

A study on the ice sheet flow was one of the main subjects of the Glaciological Research Program in Mizuho Plateau. A triangulation chain, 250 km in total length, was set up in Mizuho Plateau for this purpose. It was surveyed for the first time during a period from 24 November to 30 December 1969, by the traverse party of the 10th Japanese Antarctic Research Expedition 1968–70 (JARE-10), (NARUSE *et al.*, 1972). Resurvey of the chain was carried out four years later during a period from 20 December 1973 to 16 January 1974, by the traverse party of JARE-14 (NARUSE, 1975). A traverse survey line set up in 1970 by JARE-11 could not be resurveyed by JARE-15 during the traverse in 1974 due to the lost stakes; it is considered that most of stakes had been buried under the snow accumulated in the preceding four years.

Although the survey of a triangulation chain is a laborious work, it has two major advantages for the research of the surface flow on the far-spreading ice sheet. The first point is that one can check and correct an observational error at an individual triangle of the chain *in situ*; accordingly, the total error accumulated throughout the survey can be controlled within a much smaller value than is possible in a traverse survey. For this reason, it is possible to set up a long chain far from ice-free rocks in an inland region of the ice sheet. The second point is that one can get not only the velocities of ice flow, but also the distribution of surface strain rates of the ice sheet from the survey of the triangulation chain.

This paper describes first the methods of survey, the reduction of observed data and the calculations of velocity and strain rate of the surface ice respectively in Sections 2, 3 and 4; secondly it mentions the results and discussions in Sections 5, 6 and 7.

## 2. Method of Triangulation Survey

### 2.1. Outline of a triangulation chain

The triangulation chain stretched along the parallel of  $72^{\circ}\text{S}$  for a total distance of 250 km between A001 at the south end of the Yamato Mountains and A164 (that is S240: see Fig. A in this volume). The surface elevation of the ice sheet increases gradually along the chain from 2250 m in the vicinity of A001 to 2606 m in A164: the chain was approximately parallel to the surface contour line. The chain was composed of 164 stations, forming a series of triangles totaling 162. Configurations of the chain are illustrated in Figs. 1 and 2.

The datum point of the triangulation chain, A001, was set up on Motoi

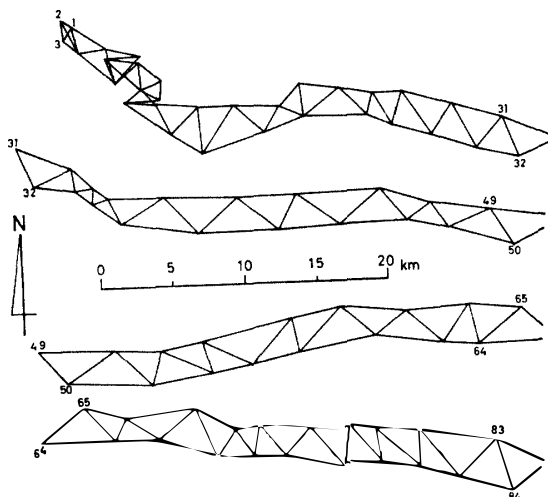


Fig. 1. Configuration of the triangulation chain from A001 to A083.

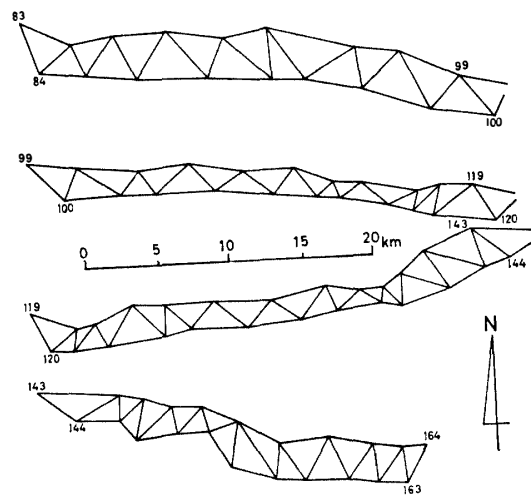


Fig. 2. Configuration of the triangulation chain from A083 to A164.

Nunatak, which belongs to the Yamato Mountains. Positions and elevations of all the triangulation stations were determined on the basis of the values of the datum point. The adopted position of this point was  $71^{\circ}47' 28.1''\text{S}$  in latitude and  $36^{\circ}12'12.2''\text{E}$  in longitude obtained by the astronomic observation carried out in 1969, and the adopted elevation was 2254 m obtained by the barometric method in 1969–1970. A base line of the chain was established between A001 and the neighboring ice-free rock A002.

The lengths of triangle sides differed considerably from place to place depending on the degree of visibility of a neighboring station on the undulating surface of the ice sheet. The minimum length was 847.34 m at the base line, the maximum was 6379 m, and the average was 2966 m.

Each station was marked by a 3-m long metal pole or a 2.5-m long bamboo stake. Twenty-two stakes among 164 stations were found missing during the resurvey in 1973–1974. These missing stakes must have been buried by heavy snow accumulation. To accomplish the continuous survey of the triangulation chain, 25 additional stations were employed bringing the total number of surveying stations to 167 in the resurvey.

## 2.2. *Angle and distance measurements*

Both the first and second surveys of the triangulation chain were conducted principally by angle measurements with Wild T2 theodolites. The horizontal angles of the three interior angles of all the constituent triangles, and the vertical angles from each station to four neighboring stations were measured. The method of survey was based nearly on the standard operating procedure for the fourth order triangulation used in Japan; namely, the limits of error allowed in angle measurements are 15 seconds as an observed differential, 25 seconds as a double angle difference, 20 seconds as a vertical angle constant difference, and 20 seconds as a closure error of a triangle. When a measured value shows an error beyond any of the above limitations, remeasurement must be made immediately.

Distance measurement with a radiowave distance meter (Cubic DM-20) and an azimuth observation by sun shot were carried out for one side of every 10th to 15th triangle to correct the accumulation of errors. The distance was measured two times for a side; the difference between the values of two measurements was in most cases smaller than

$$2 + D_m / (2 \times 10^6) \text{ cm,}$$

where  $D_m$  is the measured distance in cm. In order to prevent gross errors, the difference between the distance obtained by direct measurements and that calculated from the results of angle measurements was examined immediately during the surveys.

2.3. Procedure of survey

The field party was split into four groups, each with a theodolite and a tripod target which could be extended in height from 3.7 m to 4.7 m above the snow surface. Each group carried out measurements of horizontal and vertical angles from one station to four neighboring stations where the targets were placed upright by the other groups. After the operation was finished at a station, each group moved alternately to select the next new station in the case of the first survey, or to find out the stake of the next adjacent station in the case of the resurvey. The procedure of moving of the groups was just like the "Leapfrogging method".

The number of days when observations were impossible due to heavy driftings of snow was 10 days among 37 days in the summer of 1969 and 7 days among 28 days in the summer of 1973–1974.

3. Reduction of Observed Data

3.1. Computation of elevation

The values of distance measured by the radiowave distance meter were subjected first to meteorological correction according to air temperature and atmospheric pressure. Correction was not made for vapour pressure in the atmosphere, since the amount of water vapour is very small under the low temperature condition. Slope correction was secondly made with respect to the vertical angle so that the horizontal distance  $D_h$  between stations 1 and 2 could be obtained, as

$$D_h = D_m \cos \frac{1}{2}(\theta_1 - \theta_2), \tag{1}$$

where  $\theta_1$  is the vertical angle from station 1 to station 2 and  $\theta_2$  is that from station 2 to 1. Both  $\theta_1$  and  $\theta_2$  were measured positive upward and negative downward.

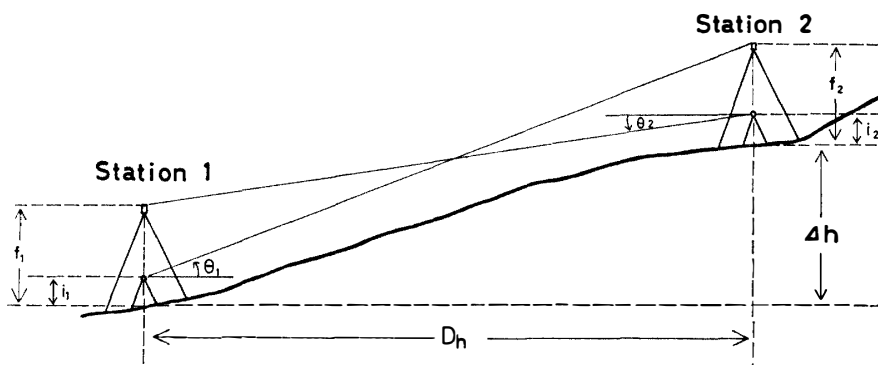


Fig. 3. A schema illustrating the method of measurement of the vertical angles  $\theta_1$  and  $\theta_2$  from both stations 1 and 2 to each other.

Elevation difference  $\Delta h$  can be calculated geometrically by using the values of  $\theta$ ,  $i$ ,  $f$  and  $D_h$ .

The difference of elevation,  $\Delta h$ , between stations 1 and 2 was calculated by the following equation, as shown by a schema in Fig. 3:

$$\Delta h = \frac{1}{2}D_h (\tan \theta_1 - \tan \theta_2) + \frac{1}{2}(i_1 + f_1) - \frac{1}{2}(i_2 + f_2), \quad (2)$$

where  $i_1$  and  $i_2$  are the height of the instrument at stations 1 and 2 respectively, and  $f_1, f_2$  the height of the target at stations 1 and 2 respectively. Possible errors resulting from the refraction by air and the curvature of the earth can be counter-balanced, because measurements of vertical angles were carried out two times from the both stations in the opposite direction and they were averaged as shown in eq. (2).

The elevation above the mean sea level of each triangulation station was obtained by accumulating the elevation differences  $\Delta h$  successively onto the elevation of a preceding station; namely, the elevations of stations  $k, k+1$  and  $k+2$  were calculated respectively by the following equations:

$$\begin{aligned} H_k &= \frac{1}{2}(H_{k-2} + \Delta h_{(k-2)k} + H_{k-1} + \Delta h_{(k-1)k}), \\ H_{k+1} &= \frac{1}{2}(H_{k-1} + \Delta h_{(k-1)(k+1)} + H_k + \Delta h_{k(k+1)}), \\ H_{k+2} &= \frac{1}{2}(H_k + \Delta h_{k(k+2)} + H_{k+1} + \Delta h_{(k+1)k}). \end{aligned} \quad (3)$$

A schematic figure of the way is illustrated in Fig. 4. The elevation of the datum point A001 was taken as 2254 m.

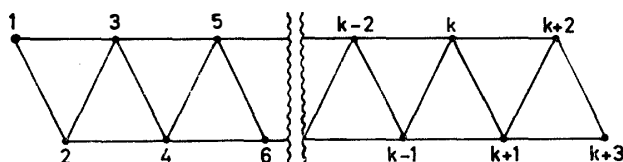


Fig. 4. A schematic figure of a part of the triangulation chain. Elevation of station  $k$  can be obtained by accumulating the elevation difference between neighbouring stations successively onto the elevation of the preceding station.

### 3.2. Computation of position

The horizontal distance between two stations,  $D_h$ , was subjected to sea-level correction, that is,

$$D_e = D_h(1 - \bar{H}/R), \quad (4)$$

where  $D_e$  is the distance on the sea level,  $\bar{H}$  the mean elevation above the sea level of two stations, and  $R$  the radius of the earth's curvature.

Positions of all triangulation stations, namely latitudes and longitudes, were calculated respectively by the observed data in 1969 and 1973–1974 by means of net-adjustment on the basis of the computer program developed by HARADA (1966). The principle of net-adjustment is to calculate every position of station

in a geodetic chain or a net with the application of the least squares method to three kinds of observation equations based on measured angle, azimuth and distance.

Let any point on the surface of the reference ellipsoid be  $P_j$ . Even if  $P_j$  is an unknown point, one can give it approximate geodetic coordinates, that is, geodetic longitude and latitude  $(\lambda_j, \phi_j)$ . In this case,  $(\lambda_j, \phi_j)$  have the corrections of small quantities  $(\delta\lambda_j, \delta\phi_j)$  as a result of net-adjustment, and then the final coordinates become  $(\lambda_j + \delta\lambda_j, \phi_j + \delta\phi_j)$ . Assumed values which correspond to the respective observations, such as angle, azimuth and distance, can be obtained geodetically by using the approximate coordinates of stations concerned. One observation equation is constructed for each observation. Input data to each observation equation are the approximate coordinates  $(\lambda_j, \phi_j)$  of unknown stations, and both assumed and observed values, while the unknown factors of the equation are the correction terms  $(\delta\lambda_j, \delta\phi_j)$ . By means of the least squares among a number of observation equations, the most probable values of geodetic coordinates of the all stations of the chain are calculated.

The triangulation chain was divided into three parts, namely A001–A049, A048–A117 and A116–A164. Computations of net-adjustment were made separately in each part. In the first part, positions of A001 and A002 were fixed as known stations; the other stations were unknown. In the second part, those of A048 and A049 were known; the others unknown. In the third part, those of A116 and A117 were known; the others unknown. Computations were repeated three or four times in each of the three parts of the chain by using the calculated values of the positions of stations in lieu of the approximate values of the latitudes and longitudes, until the correction terms to them become negligibly small.

A reference ellipsoid used in the calculation was Bessel's ellipsoid; namely, the radius of equator is 6377397 m and the flattening of the earth is 1/299.15.

#### 4. Calculation of Flow Vector and Strain

##### 4.1. Horizontal velocity of ice flow

The horizontal vector of ice movement was calculated at each triangulation station from the difference between two geodetic positions in 1969 and 1973–1974 which were obtained by net-adjustments. The horizontal displacement  $\Delta S$  and its direction  $\beta$  indicated by the azimuth clockwise from the north point were given as follows:

$$\Delta S = \sqrt{(p\Delta\phi)^2 + (q\Delta\lambda)^2}, \quad (5)$$

$$\beta = \tan^{-1}(q\Delta\lambda/p\Delta\phi), \quad (6)$$

where  $\Delta\phi$  and  $\Delta\lambda$  are respectively the difference of the latitudes and longitudes

of the station between two measurements in 1969 and 1973–1974,  $p$  the coefficient which is almost constant, and  $q$  the coefficient which varies with the latitude of the station.

Results of calculations on displacement, azimuth and time interval in days between two measurements are tabulated in JARE Data Reports (NARUSE, 1975) at a total of 141 stations. From the data, the surface velocities of ice flow in m/year can be obtained. The velocities which are to be shown in the following sections are not the values on the surface of the ice sheet, but on the surface of the reference ellipsoid; for example, the value of 20 m/year on the ellipsoid corresponds to 20.008 m/year on the surface of 2500 m in elevation.

#### 4.2. Vertical component of ice flow velocity

The surface elevations of the ice sheet in 1969 and 1973–1974 were respectively calculated at each surveying station along the chain. The vertical displacement of the surface snow, namely displacement of the top of the stake, was obtained by subtracting the thickness of net accumulation of snow for a period of four years from the difference of the above two surface elevations. The results are also tabulated in JARE Data Reports (NARUSE, 1975).

The “emergence velocity” or “submergence velocity” of the ice flow was

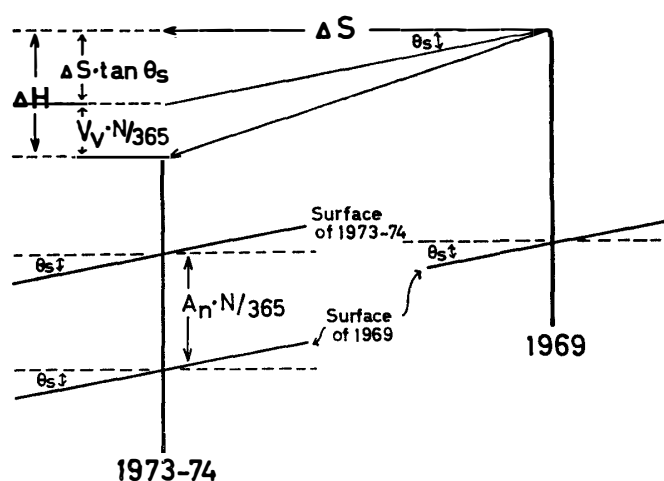


Fig. 5. A schematic figure showing the movement of a pole in the period from 1969 to 1973–1974.

- $\Delta S$ : Horizontal displacement during the period,
- $\Delta H$ : Vertical displacement during the period,
- $V_v$ : Emergence or submergence velocity per year; it is called vertical velocity in this paper,
- $A_n$ : Annual net accumulation of snow,
- $\theta_s$ : Surface slope,
- $N$ : Number of days between two observations.

The values of  $\theta_s$ ,  $\Delta H$ ,  $V_v$  and  $A_n$  are measured positive upward. The diagram refers to the region of “submergence flow”.

given by taking into account the surface slope. This velocity is called the vertical velocity  $V_v$  in this paper. Fig. 5 shows the location of a stake set up in the snow surface in 1969 and its location in 1973–1974. The diagram refers to the accumulation area as most parts of the triangulation chain. The horizontal displacement  $\Delta S(m)$  and the vertical displacement  $\Delta H(m)$  of the stake were measured with respect to a fixed coordinate system located on the earth. The horizontal component of the flow velocity  $V_h(m/year)$  is  $\Delta S \cdot 365/N$ , where  $N$  is the number of days between two observations. If the ice flow was parallel to the surface,  $\Delta H$  would be equal to  $\Delta S \tan \theta_s$ , where  $\theta_s$  is the surface slope. But the ice flow is in this case downward relative to the surface, so the absolute value of the vertical displacement  $\Delta H$  is larger than  $\Delta S \tan \theta_s$  by an amount of the vertical velocity  $V_v(m/year)$ ; namely,

$$\begin{aligned} -\Delta H &= -\Delta S \tan \theta_s - V_v \cdot N/365, \\ V_v &= (\Delta H - \Delta S \tan \theta_s) 365/N = \Delta H' - V_h \tan \theta_s, \end{aligned} \quad (7)$$

where  $\Delta H'$  is the vertical displacement of the top of the stake per year, that is  $\Delta H \cdot 365/N$ . Values of  $\Delta H$ ,  $\Delta H'$ ,  $V_v$  and  $\theta_s$  are measured positive upward in this paper. As for the component  $V_p$  perpendicular to the surface, it becomes more important in the discussion of the mass balance at a station, which is deduced from the vertical flow as shown in Section 6. It is obtained as

$$V_p = V_v \cos \theta_s = \Delta H' \cdot \cos \theta_s - V_h \sin \theta_s. \quad (8)$$

However, since the value of the surface slope was smaller than one degree all over the area along the triangulation chain,  $V_p$  is approximately equal to  $V_v$ .

Distribution of vertical velocities along the chain is to be shown and discussed in Section 6.

#### 4.3. Mean square error of velocity

Mean square error in geodetic coordinates, namely in latitude and longitude, was calculated at each triangulation station as the results of net-adjustment of the chain. Latitudes, longitudes and their mean square errors at every ten stations along the chain are tabulated in Table 1, separately in the first survey of 1969 and the second survey of 1973–1974. Because the triangulation chain stretched along the parallel, that is from west to east, the errors in longitude were given to be larger values than errors in latitude. The maximum error was obtained at A164 which was the farthest station from the datum point A001; mean square error in position at A164 was 3.42 m in the first survey and 5.62 m in the second survey.

The horizontal displacement of surface flow  $\Delta S$  and its direction  $\beta$  were calculated by eqs. (5) and (6) mentioned in the foregoing section. Absolute value of the surface velocity was obtained as  $\Delta S$  divided by the time interval between

Table 1. Horizontal flow velocity and its mean square error at every ten station of a triangulation chain.

Station	Latitude (S)	Longitude (E)	1st survey		2nd survey		$V_h$ (m/year)	$E_s$ (m/year)	$\beta$ (degree)	$E_\beta$ (degree)
			$E_{lat}$ (m)	$E_{lon}$ (m)	$E_{lat}$ (m)	$E_{lon}$ (m)				
A005	71°48'24"	36°16'13"	0.05	0.05	0.12	0.17	0.4	0.03	342	6.2
015	71 51 45	36 23 18	0.30	0.26	0.34	0.36	1.1	0.11	313	5.8
025	71 50 31	36 47 42	0.52	0.92	0.83	1.20	4.1	0.25	347	5.2
035	71 53 12	37 12 08	0.69	1.07	1.29	1.76	4.5	0.37	12	6.4
045	71 53 23	37 46 02	1.13	1.57	1.86	3.12	9.0	0.55	6	5.4
055	71 54 28	38 18 39	1.21	1.73	2.19	3.78	15.1	0.64	9	3.8
065	71 54 16	38 56 57	1.34	1.96	2.31	3.96	20.4	0.67	1	3.0
075	71 55 18	39 23 45	1.40	2.06	2.54	4.17	20.7	0.73	0	3.2
085	71 56 55	39 51 54	1.56	2.26	2.61	4.21	19.3	0.76	359	3.5
095	71 56 54	40 25 53	1.62	2.30	2.74	4.35	18.5	0.80	354	3.7
105	71 58 16	40 57 46	1.82	2.35	2.81	4.40	17.5	0.85	352	3.9
115	72 00 00	41 24 28	2.00	2.47	2.99	4.55	16.6	0.91	350	4.3
125	71 59 51	41 43 07	2.02	2.49	2.98	4.56	14.8	0.92	349	4.8
135	71 59 43	42 10 34	2.07	2.58	3.02	4.66	14.4	0.94	348	5.1
145	71 57 59	42 33 56	2.10	2.64	3.04	4.68	14.7	0.97	343	5.0
155	72 01 24	42 52 04	2.13	2.66	3.06	4.70	13.3	0.99	341	5.5
164	72 00 07	43 09 48	2.14	2.67	3.08	4.70	13.6	1.01	336	5.2

$E_{lat}$ : Mean square error in latitude of a station expressed by meter.

$E_{lon}$ : Mean square error in longitude of a station expressed by meter.

$V_h$ : Horizontal velocity of ice flow.

$E_s$ : Mean square error of horizontal velocity.

$\beta$ : Azimuth of horizontal velocity measured clockwise from north.

$E_\beta$ : Mean square error of azimuth.

two observations. Applying the theory of propagation of error to these equations, mean square errors in velocity and in azimuth were calculated, and are shown in Table 1. Since the surface flow is almost in the direction from south to north, the mean square error in horizontal velocity was strongly controlled by the error involved in latitude, not by the error in longitude. Relative error of surface velocity was in a range from 3% to 10%. The mean square error in azimuth was, on the contrary, controlled rather by the error in longitude. The errors in direction showed, therefore, relatively large values such as 3 to 6 degrees.

Mean square error in surface elevation was estimated at each triangulation station by applying also the theory of propagation of error to eq. (3), from which the surface elevations were calculated. The errors at every ten stations along the chain are tabulated in Table 2 with the relative elevations of stations. As noted in Table 2, the tendency of the accumulation of errors was almost the

Table 2. Relative elevation, vertical velocity and their mean square errors at every ten stations of a triangulation chain.

Station	1st survey		2nd survey		$V_v$ (m/year)	$E_v$ (m/year)
	$H$ (m)	$E_h$ (m)	$H$ (m)	$E_h$ (m)		
A005	27.38	0.06	27.51	0.13	+0.09	0.04
015	99.13	0.11	99.20	0.22	+0.07	0.06
025	123.30	0.23	123.36	0.28	-0.02	0.09
035	169.43	0.31	168.89	0.32	-0.06	0.11
045	145.58	0.34	145.79	0.38	-0.15	0.13
055	151.92	0.41	150.86	0.43	-0.13	0.15
065	131.27	0.45	128.56	0.52	-0.71	0.18
075	160.52	0.54	157.23	0.55	-0.92	0.20
085	192.01	0.61	188.50	0.57	-0.78	0.22
095	201.71	0.63	197.35	0.63	-0.93	0.23
105	231.72	0.71	227.56	0.67	-1.03	0.25
115	259.82	0.75	255.66	0.69	-1.02	0.26
125	285.54	0.79	281.97	0.72	-0.78	0.27
135	272.35	0.81	269.28	0.78	-1.08	0.28
145	289.89	0.84	286.47	0.80	-0.82	0.29
155	337.39	0.85	334.11	0.83	-0.77	0.30
164	354.83	0.88	352.20	0.84	-0.64	0.31

$H$ : Relative elevation of a station to elevation of A001(=0.0m).

$E_h$ : Mean square error of relative elevation.

$V_v$ : Vertical velocity.

$E_v$ : Mean square error of vertical velocity.

same between the first survey of 1969 and the second survey of 1973–1974. Relative error in surface elevation was in a range from 0.1% to 0.35%.

The vertical velocity  $V_v$  was calculated from eq. (7). Assuming the error in the surface slope  $\theta_s$  as 10 min ( $\sim 1/350$ ), the mean square error involved in  $V_v$  was obtained at each station, and is shown in Table 2. Relative error in the vertical velocity was considerably larger such as 100% in the region from A003 to around A060 where the vertical velocity was very small. While in the region eastward from A060, relative errors showed rather small values from 22% to 48%.

#### 4.4. Surface deformation of the ice sheet

The square strain grids of 1 km in each side were installed separately at nine stations over Mizuho Plateau in 1969–1970 (NARUSE *et al.*, 1972). Seven of them were resurveyed during the period from 1970 to 1975 (SATOW, 1977). Locations of these strain grids and the results of strain rates are described in another article by NARUSE and SHIMIZU (1978).

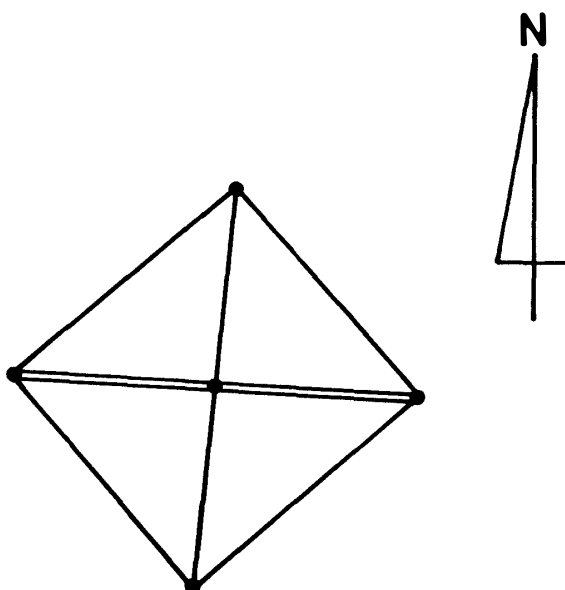


Fig. 6. Configuration of a five-stake strain grid at Mizuho Camp.

*Distance measurement was made of a diagonal shown by a double line.*

Two types of square strain grids were actually set up: the four-stake grid and the five-stake grid. The former had a stake at each corner of a square with a side approximately 1 km long, whereas the latter had another additional stake at the cross point of two diagonals as illustrated in Fig. 6. The length of one diagonal was measured with a radiowave distance meter (Cubic DM-20) and each interior angle of the constituent triangles with Wild T2 theodolites. Methods of observations and data corrections are the same as those of the triangulation chain mentioned in the foregoing section.

A five-stake grid was set up not only to measure deformation of the square but also to check the homogeneous strain in the wide area of approximately 1 km<sup>2</sup>. If the mode of strain is homogeneous, all straight lines in the square remain straight and parallel sides of the square parallel after deformation. These checks were made with the five-stake grid at Mizuho Camp. Result of surface deformation for the period of four years showed that the extension of the 1 km long side was 41 cm in maximum, and the contraction of the side of the same length was 174 cm in maximum. While the deviation of the central stake from each of the two diagonals after four years' deformation was respectively 7 cm and 13 cm; the deviation of each of the parallel sides four years later was respectively 4 seconds and 34 seconds; namely, the deviation of 34 seconds corresponds to the length of 16 cm at the point of 1 km in distance. The above results indicate that

Table 3. Calculated values of strain parameters of the ice sheet surface at each triangle of the triangulation chain. Explanations of the symbols are given in the text.

Triangle	$\alpha$ (degree)	$\dot{\epsilon}_1$ $\times 10^{-4}$ (1/year)	$\dot{\epsilon}_2$ $\times 10^{-4}$ (1/year)	$\dot{\gamma}$ $\times 10^{-4}$ (1/year)	$\dot{\gamma}_{\max}$ $\times 10^{-4}$ (1/year)	$\dot{\omega}$ (degree/ year)	$\dot{\epsilon}_3$ $\times 10^{-4}$ (1/year)
1. 2. 3	97.34	+0.46	-1.49	-1.02	1.95	+0.005	
1. 2. 4	100.54	+0.51	-2.15	-1.64	2.66	+0.006	
1. 3. 4	86.45	+0.50	-1.70	-1.20	2.20	+0.003	
1. 4. 5	71.00	-0.03	-1.63	-1.66	1.60	0	
2. 3. 4	81.85	+0.48	-1.39	-0.92	1.87	+0.002	
4. 5. 6	61.28	+0.09	-1.39	-1.30	1.48	+0.001	+0.40
5. 6. 7	54.33	-0.28	-1.46	-1.74	1.17	+0.001	+0.52
6. 7. 8	54.76	-0.27	-1.64	-1.91	1.38	0	+0.66
6. 8. 9	56.52	-0.43	-1.61	-2.04	1.18	+0.001	+0.53
6. 10. 13	34.60	+1.10	-0.93	+0.17	2.04	+0.006	
8. 9. 10	35.62	-0.03	-1.20	-1.23	1.17	0	+0.54
9. 10. 11	40.64	+0.58	-1.76	-1.18	2.34	-0.003	+0.53
10. 11. 12	24.40	+1.69	-1.57	+0.17	3.26	0	+0.73
10. 12. 13	42.84	+0.97	-1.59	-0.62	2.57	+0.006	+0.73
10. 13. 14	36.78	+1.04	-0.80	+0.24	1.84	+0.006	
11. 14. 16	26.37	+2.08	-0.53	+1.55	2.62	-0.001	
13. 14. 15	86.08	-0.31	-1.00	-1.31	0.69	+0.002	+0.70
14. 15. 16	53.96	+0.45	-1.05	-0.59	1.50	-0.001	+0.59
15. 16. 17	55.65	+0.48	-1.73	-1.25	2.21	-0.002	+0.57
16. 17. 18	49.51	+1.10	-2.45	-1.36	3.55	-0.006	+0.61
17. 18. 19	52.22	+1.03	-0.70	+0.33	1.73	-0.004	+0.57
18. 19. 20	27.80	+6.56	-1.36	+5.19	7.91	-0.018	+0.38
18. 20. 22	42.53	+3.15	-2.09	+1.05	5.24	-0.021	
19. 20. 21	16.00	+7.16	-1.81	+5.34	8.96	-0.008	+0.21
20. 21. 22	15.29	+4.65	-1.77	+2.88	6.41	-0.006	+0.09
21. 22. 23	174.81	+3.82	+0.02	+3.85	3.80	+0.006	+0.10
21. 23. 24	29.79	+1.37	-0.48	+0.89	1.84	0	
23. 24. 25	42.06	+0.44	-0.33	+0.10	0.77	+0.003	-0.08
24. 25. 26	62.01	+0.77	-0.14	+0.62	0.91	+0.002	
25. 26. 27	177.14	+0.35	-1.98	-1.63	2.33	-0.004	-0.12
26. 27. 28	144.56	+0.78	-0.32	+0.46	1.10	-0.005	-0.71
27. 28. 29	142.49	+0.78	-0.63	+0.16	1.41	-0.004	-0.97
28. 29. 30	127.90	+1.31	-0.49	+0.82	1.80	-0.006	-1.04
29. 30. 31	104.08	+2.90	-0.55	+2.35	3.45	0	
30. 31. 32	88.58	+1.37	-0.88	+0.49	2.25	+0.001	-0.63
31. 32. 33	81.43	+1.75	-0.74	+1.02	2.49	0	-0.67
32. 33. 34	88.64	+1.98	-0.77	+1.21	2.76	-0.002	-1.11

Table 3. (Continued)

Triangle	$\alpha$ (degree)	$\dot{\epsilon}_1$ $\times 10^{-4}$ (1/year)	$\dot{\epsilon}_2$ $\times 10^{-4}$ (1/year)	$\dot{A}$ $\times 10^{-4}$ (1/year)	$\dot{\gamma}_{\max}$ $\times 10^{-4}$ (1/year)	$\dot{\omega}$ (degree/ year)	$\dot{\epsilon}_3$ $\times 10^{-4}$ (1/year)
33. 34. 35	77.78	+4.03	-0.76	+3.26	4.79	-0.006	-1.14
34. 35. 36	74.67	+4.04	+0.97	+5.02	3.07	-0.005	-0.81
35. 36. 37	61.07	+3.18	+0.51	+3.68	2.67	-0.006	-0.48
36. 37. 38	51.48	+3.50	+0.03	+3.53	3.46	-0.002	-0.52
37. 38. 39	40.07	+2.70	-0.32	+2.37	3.02	-0.004	-0.83
38. 39. 40	42.46	+2.66	-0.86	+1.79	3.52	-0.004	-0.92
39. 40. 41	36.04	+2.79	-0.99	+1.80	3.79	-0.007	
40. 41. 42	37.25	+2.81	-2.47	+0.34	5.28	-0.006	
41. 42. 43	37.25	+3.06	-2.46	+0.59	5.52	-0.006	
42. 43. 44	27.67	+2.84	-1.08	+1.75	3.92	0	-1.58
43. 44. 45	19.62	+1.56	-1.22	+0.35	2.78	-0.001	-1.55
44. 45. 46	8.21	+2.36	-1.10	+1.26	3.46	+0.002	-1.24
45. 46. 47	14.57	+2.47	-0.58	+1.89	3.05	+0.003	-0.96
46. 47. 49	55.06	+1.19	-0.70	+0.49	1.89	-0.005	-0.38
49. 51. 52	71.92	+1.81	-2.15	-0.34	3.96	-0.008	+0.43
51. 52. 53	48.51	+6.17	-1.52	+4.64	7.69	-0.016	+0.30
52. 53. 54	36.99	+5.19	-3.78	+1.40	8.97	-0.012	-0.10
53. 54. 55	33.94	+5.03	-3.68	+1.35	8.71	-0.015	-0.47
54. 55. 56	35.40	+5.24	-3.42	+1.81	8.66	-0.015	-0.67
55. 56. 57	44.39	+2.41	-3.74	-1.33	6.15	-0.011	-0.74
56. 57. 60	19.10	+3.40	-1.47	+1.92	4.87	-0.001	-0.58
57. 59. 60	21.56	+3.37	-1.37	+2.00	4.74	0	-0.62
59. 60. 61	22.92	+3.02	-1.22	+1.80	4.23	+0.002	-0.76
60. 61. 62	28.14	+2.55	-0.96	+1.59	3.50	-0.001	-1.02
61. 62. 63	22.13	+2.10	-1.15	+0.94	3.24	-0.002	-1.02
62. 63. 64	25.65	+1.98	-0.29	+1.69	2.27	-0.004	-1.25
63. 64. 65	17.02	+1.92	-1.53	+0.39	3.45	-0.006	-1.32
64. 65. 66	8.32	+2.17	-0.76	+1.42	2.93	-0.007	-2.46
65. 66. 67	10.16	+2.88	-1.03	+1.85	3.92	-0.010	-2.81
66. 67. 68	175.46	+3.49	-0.06	+3.43	3.55	-0.007	-3.51
67. 68. 69	173.62	+3.07	+0.05	+3.12	3.02	-0.005	-3.53
68. 69. 70	171.13	+3.35	+0.11	+3.46	3.24	-0.005	-3.80
69. 70. 71	175.65	+3.44	+0.66	+4.10	2.78	-0.006	-4.05
70. 71. 72	172.70	+3.63	+0.74	+4.37	2.89	-0.005	-4.01
71. 72. 73	162.52	+3.32	+0.33	+3.65	2.99	-0.003	-4.19
72. 73. 75	169.74	+3.28	-1.63	+1.65	4.92	-0.001	-4.28
72. 75. 76	171.56	+2.79	-1.77	+1.01	4.56	-0.001	-4.36
75. 76. 77	169.77	+2.40	-1.10	+1.31	3.50	+0.002	-4.41
76. 77. 78	168.62	+2.41	-0.82	+1.59	3.22	+0.002	-4.32

Table 3. (Continued)

Triangle	$\alpha$ (degree)	$\dot{\epsilon}_1$ $\times 10^{-4}$ (1/year)	$\dot{\epsilon}_2$ $\times 10^{-4}$ (1/year)	$\dot{A}$ $\times 10^{-4}$ (1/year)	$\dot{\gamma}_{\max}$ $\times 10^{-4}$ (1/year)	$\dot{\omega}$ (degree/ year)	$\dot{\epsilon}_3$ $\times 10^{-4}$ (1/year)
77· 78· 79	178.26	+2.74	-0.05	+2.68	2.79	+0.002	-4.10
78· 79· 80	0.70	+2.76	+0.07	+2.84	2.69	+0.001	-3.82
79· 80· 81	177.92	+2.42	+0.16	+2.57	2.26	+0.002	-3.48
80· 81· 82	177.58	+2.42	+0.65	+3.06	1.77	+0.002	-3.61
81· 82· 83	173.69	+2.52	+0.02	+2.54	2.50	+0.001	-3.55
82· 83· 84	175.18	+2.25	+0.10	+2.35	2.14	0	-3.97
83· 84· 85	177.96	+2.30	+0.11	+2.41	2.18	-0.001	-4.20
84· 85· 86	10.77	+1.80	-0.35	+1.45	2.15	-0.001	-4.26
85· 86· 87	12.47	+1.85	-0.27	+1.58	2.12	-0.001	-4.23
86· 87· 89	9.05	+2.25	-1.48	+0.76	3.73	+0.003	-4.22
86· 89· 90	4.55	+1.76	-1.00	+0.76	2.76	0	-4.71
89· 90· 92	166.40	+0.68	-1.22	-0.54	1.89	+0.003	-4.68
92· 94· 95	153.47	+2.99	-0.60	+2.39	3.58	-0.001	-4.35
94· 95· 96	151.46	+2.86	-0.56	+2.29	3.41	-0.001	-4.52
95· 96· 97	151.13	+2.83	-0.21	+2.62	3.04	-0.002	-4.90
96· 97· 98	161.44	+1.99	-0.48	+1.51	2.48	-0.001	-5.12
97· 98· 99	170.35	+2.23	-0.42	+1.80	2.65	-0.004	-5.08
98· 99· 100	171.20	+2.35	-0.60	+1.75	2.95	-0.003	-4.88
99· 100· 101	171.46	+2.33	-0.50	+1.82	2.83	-0.002	-4.64
100· 101· 102	174.23	+2.25	-0.75	+1.49	3.00	-0.002	-4.72
101· 102· 103	175.74	+2.06	-0.62	+1.45	2.68	-0.001	-4.91
102· 103· 105	163.66	+2.99	-0.24	+2.76	3.22	0	-4.88
105· 107· 108	8.23	+1.28	-0.06	+1.22	1.34	+0.002	-4.89
107· 108· 109	4.02	+1.52	-0.35	+1.17	1.86	+0.001	-5.12
108· 109· 110	0.25	+1.62	-0.22	+1.40	1.84	+0.001	-5.37
109· 110· 111	176.12	+1.41	-0.08	+1.34	1.49	+0.002	
110· 111· 112	179.50	+1.27	-0.13	+1.14	1.40	+0.002	
111· 112· 113	168.99	+1.22	-0.31	+0.91	1.53	+0.003	
112· 113· 114	179.08	+0.93	-0.48	+0.45	1.41	+0.004	
113· 114· 115	9.48	+0.84	0.00	+0.83	0.84	+0.006	
114· 115· 116	160.89	+2.44	+0.18	+2.62	2.26	+0.003	-6.58
115· 116· 117	160.44	+2.86	-0.30	+2.56	3.16	+0.006	-5.81
116· 117· 118	153.69	+1.97	-0.10	+1.87	2.07	+0.003	-5.64
117· 118· 120	161.04	+1.84	-0.55	+1.29	2.39	+0.004	-5.40
117· 120· 121	160.47	+1.66	-0.30	+1.36	1.97	+0.005	
120· 121· 122	142.18	+3.78	-0.09	+3.69	3.87	+0.002	
121· 122· 123	142.96	+4.00	-0.39	+3.61	4.38	+0.004	
123· 125· 126	137.44	+2.58	-0.11	+2.47	2.68	-0.001	-4.32
125· 126· 127	141.28	+2.59	+0.72	+3.31	1.87	-0.001	

Table 3. (Continued)

Triangle	$\alpha$ (degree)	$\dot{\epsilon}_1$ $\times 10^{-4}$ (1/year)	$\dot{\epsilon}_2$ $\times 10^{-4}$ (1/year)	$\dot{J}$ $\times 10^{-4}$ (1/year)	$\dot{\gamma}_{\max}$ $\times 10^{-4}$ (1/year)	$\dot{\omega}$ (degree/ year)	$\dot{\epsilon}_3$ $\times 10^{-4}$ (1/year)
126·127·128	149.24	+2.30	+0.58	+2.88	1.72	-0.002	
127·128·129	151.13	+2.38	0.00	+2.38	2.38	-0.003	
128·129·130	158.91	+1.95	-0.19	+1.76	2.13	-0.003	-4.32
129·130·131	155.17	+1.86	-0.41	+1.45	2.28	-0.002	
130·131·133	171.51	+1.06	-0.81	+0.25	1.88	-0.002	
130·133·138	9.05	+0.86	-1.45	-0.59	2.32	+0.001	-5.81
133·138·141	173.59	+0.46	-1.80	-1.33	2.26	-0.001	
138·140·141	0.55	+0.27	-2.18	-1.91	2.45	-0.002	
140·141·142	19.43	+0.25	-0.85	-0.59	1.10	+0.002	
141·142·144	141.32	+0.44	-1.34	-0.91	1.78	+0.006	
141·144·145	125.04	+0.06	-0.74	-0.69	0.80	+0.003	
144·145·146	128.10	+2.05	-0.45	+1.60	2.49	-0.004	
145·146·147	131.27	+1.72	-0.46	+1.27	2.18	-0.004	
146·147·148	136.60	+2.62	-0.42	+2.20	3.05	-0.003	
147·148·149	137.73	+2.36	-0.39	+1.98	2.75	-0.004	
148·149·154	166.29	+1.08	-0.83	+0.25	1.90	0	
149·151·154	164.12	+0.87	-0.20	+0.66	1.07	+0.002	
151·154·155	154.97	+0.89	-1.87	-0.98	2.77	+0.004	
151·155·157	165.05	+1.62	-3.19	-1.57	4.81	-0.003	
151·157·160	171.26	+1.43	-1.82	-0.39	3.25	+0.001	
157·159·160	174.96	+0.73	-1.86	-1.13	2.59	+0.001	-4.46
159·160·161	140.52	+1.33	-0.44	+0.89	1.77	-0.004	-3.35
160·161·162	123.07	+1.62	+0.23	+1.85	1.39	-0.005	
161·162·163	135.97	+1.38	+0.19	+1.57	1.19	-0.003	
162·163·164	111.25	+1.24	+0.85	+2.09	0.39	-0.005	

two straight diagonals each aligned on three stakes in the unstrained state remained almost straight and two pairs of the parallel sides remained almost parallel after straining. Consequently, the homogeneous strain on the scale of 1 km holds approximately in the area around Mizuho Camp.

Therefore, the surface deformation of the ice sheet was calculated on each triangle of the chain, assuming that the strain was homogeneous on the scale of the triangle over the surveyed region. Method of calculation of strain rates was to get the rate of transformation of a circumscribed circle about a triangle into an ellipse caused by a finite homogeneous strain (JAEGER, 1969). Geodetic coordinates of three points of each triangle were obtained both in 1969 and 1973-1974, by the net-adjustment of the chain. If the amount of the translation was subtracted from the displacement of a triangle, pure strain and rotation of

the ice sheet surface can be calculated: the former specifies the shape of the strain ellipse, while the latter gives the rotation of principal axes of strain. Taking a radius of the circumscribed circle about an initial triangle as unity, and lengths of major and minor axes of the strain ellipse as  $2F$  and  $2G$ , the parameters of the ice deformation can be represented as the function of  $F$  and  $G$ . As the results of calculations to determine the values of  $F$  and  $G$  from the coordinates of the points of a triangle concerned, the following strain rate parameters were obtained and are shown in Table 3:

$\alpha$ : Direction of the principal axis of strain  $\varepsilon_1$  (see below), indicated by the azimuth from  $0^\circ$  to  $180^\circ$  in turn ( $0^\circ$ : North;  $90^\circ$ : East;  $180^\circ$ : South).

$\dot{\varepsilon}_1, \dot{\varepsilon}_2$ : Principal strain rate per year, obtained by  $\varepsilon_1 = F - 1$  and  $\varepsilon_2 = G - 1$ . The positive sign indicates tension and the negative sign a compression. Strain  $\varepsilon_1$  signifies the algebraically maximum value among the strains in the whole directions;  $\varepsilon_2$  the algebraically minimum value.

$\dot{A}$ : Rate of the change of area of a triangle per year, namely dilatation, obtained by  $\dot{A} = FG - 1$ .

$\dot{\gamma}_{\max}$ : Maximum shear strain rate per year, obtained by  $\dot{\gamma}_{\max} = (F^2 - G^2) / 2FG$ . The directions of it are  $\alpha \pm 45^\circ$ .

$\dot{\omega}$ : Rate of rotation clockwise of the principal axes per year, obtained by  $\dot{\omega} = \alpha' - \alpha$ , where  $\alpha'$  is a direction of a major axis of strain ellipse.

Observed error in each length of a side was estimated to be smaller than 4 cm, which gave mean square error of strain rate smaller than  $10^{-5}$  per year.

## 5. Distribution of Horizontal Flow Velocity and Surface Strain

### 5.1. Distribution of flow vector and principal strain

Horizontal flow vectors and the principal strains of the snow or ice surface along the triangulation chain were distributed as shown by arrows in Figs. 7, 8, 9 and 10, with the topographic contours of the surface relief. The 10-m interval contour lines are based on the results of triangulation survey and observation of surface slopes of the ice sheet as mentioned in Section 7.

Remarkable features of the distribution of flow and strain are summarized as follows:

(a) Flow rates had very small values less than 2 m/year and the flow direction was northwestward in the vicinity of the Yamato Mountains, namely the region from A003 to A020 (see Fig. 7). It is considered that the ice flow was slowed by the effect of existence of many nunataks downstream of this part of the measurement area. As a consequence, the mode of ice deformation was longitudinally compressive as seen in the pattern of the principal strains in Fig. 7.

This region has larger undulation of the surface relief compared with other

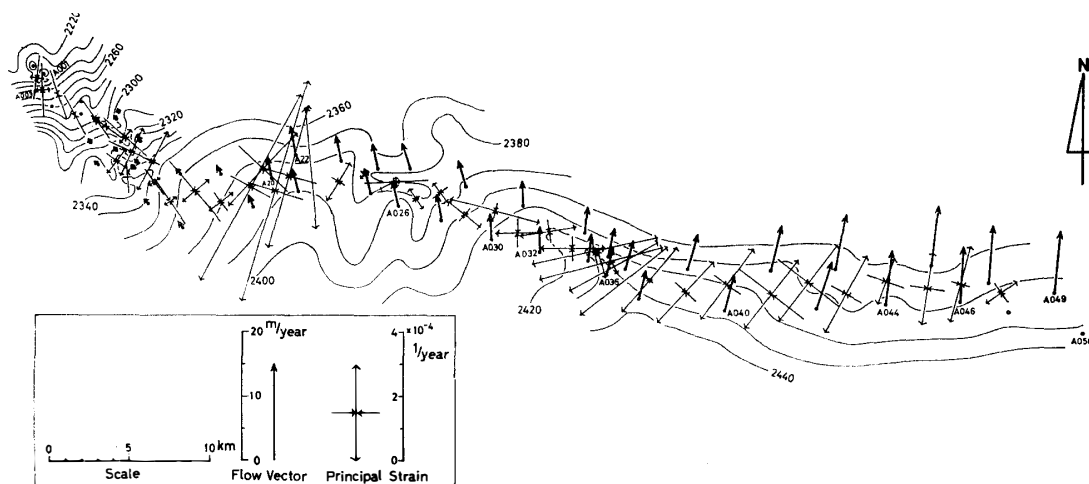


Fig. 7. Distribution of horizontal vectors of ice flow and principal strains in the region from A001 to A049.

regions along the chain. The surface of the ice sheet was not covered with snow but was composed of ice, as a result of negative net accumulation of 2–7 cm in ice thickness per year (YOKOYAMA, 1975). A large number of meteorites were found (YOSHIDA *et al.*, 1971; SHIRAISHI *et al.*, 1976; YANAI, 1976) in this region which, therefore, was named the Meteorite Ice Field.

(b) Large tensile strains along the direction from SSW to NNE were noted near A020 (see Fig. 7). The fact is compatible with the existence of the large-scale crevasses which run along the direction from WNW to ESE.

(c) The direction of ice flow was different on either side of A032 at  $37^\circ\text{E}$

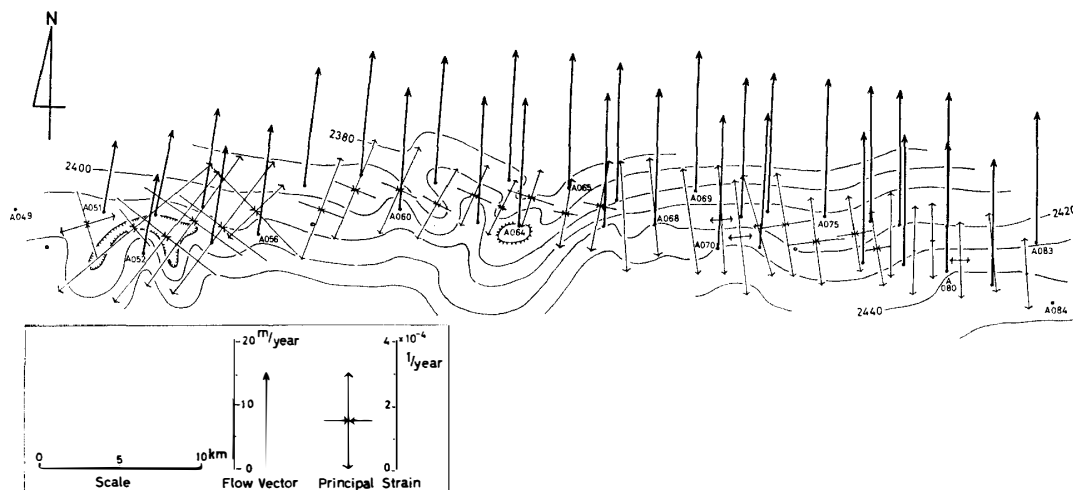


Fig. 8. Distribution of horizontal vectors of ice flow and principal strains in the region from A050 to A083.

in longitude (see Fig. 7). To the west of the boundary, the flow has a westerly component, and to the east it has an easterly component. The macro-scale surface contours of the ice sheet showed a ridge there (SHIMIZU *et al.*, 1978). It must follow, therefore, that the ice divide between the drainage of Shirase Glacier and the drainage at its westside exists near 37°E.

(d) The absolute value of flow velocity increased gradually with the increase of the station number, that is from west to east (see Fig. 7). It was more than 10 m/year at A051 and more than 20 m/year in the region between A065 and A081 (see Fig. 8). The maximum value was observed to be 21.3 m/year at A069 (39°10'E).

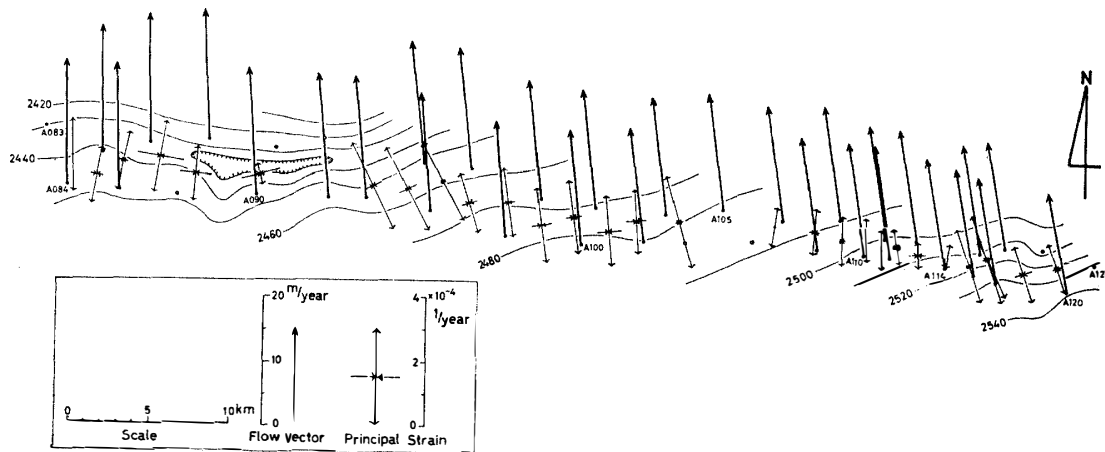


Fig. 9. Distribution of horizontal vectors of ice flow and principal strains in the region from A084 to A120.

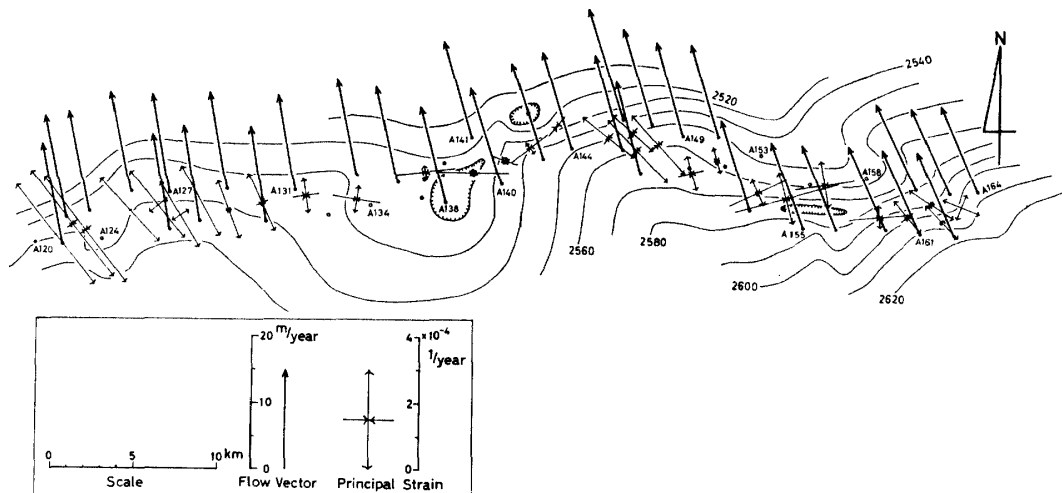


Fig. 10. Distribution of horizontal vectors of ice flow and principal strains in the region from A121 to A164.

(e) The value of velocity decreased slightly starting at A070 (see Fig. 8), and reached 13.6 m/year at A164 which was located at the east end of the triangulation chain (see Fig. 10).

(f) The direction of the ice flow pointed slightly eastward from north in the region from A033 to A075 (see Figs. 7 and 8) and slightly westward in the region from A076 eastward (see Figs. 8 and 9). The direction shifted gradually westward in the eastern part of the chain, and finally it was NNW at A164 (see Fig. 10).

(g) The direction and magnitude of the principal strains varied somewhat by the effect of the distinct surface undulation as seen around the surface depressions at A138 or A156 (see Fig. 10). However, the direction of the maximum extension was rather close to that of the surface flow.

### 5.2. Variation of flow velocity, dilatation and maximum shear strain

Fig. 11 shows the variations of the horizontal component of flow velocity, the rate of surface dilatation and the rate of maximum shear strain plotted against

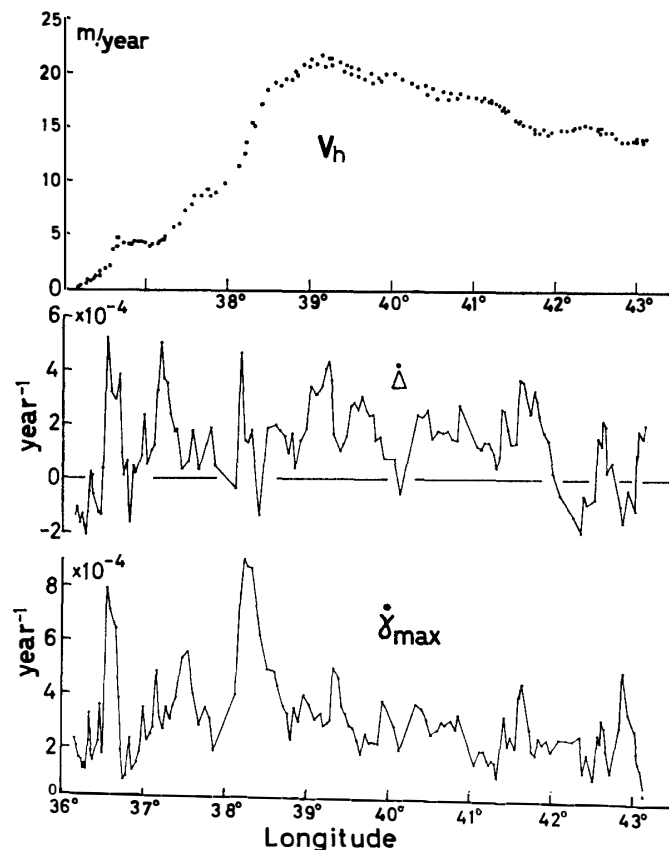


Fig. 11. Variations of the horizontal component of velocity  $V_h$  in m/year, the rate of the surface dilatation  $\dot{\Delta}$  in 1/year, and the rate of the maximum shear strain  $\dot{\gamma}_{\max}$  in 1/year.

the longitude from  $36^{\circ}10'E$ , the east end of the Yamato Mountains, to  $43^{\circ}10'E$ .

The spatial pattern of variation of the absolute value of velocity which was mentioned in the foregoing section in (a), (b) and (e), is more clearly shown in Fig. 11. A strong eastward increase in velocity magnitude exists in the region between  $37^{\circ}20'E$  and  $38^{\circ}30'E$ ; eastward from  $39^{\circ}10'E$  there is a gradual decrease of velocity. A slight scattering of values found around  $39^{\circ}$ – $41^{\circ}E$  signifies the difference of velocities between the north-side line and the south-side line of the triangulation chain: velocity in the north side was higher than in the south side up to the value of several tens of centimeters per year. It follows that the ice flow was tensile along the direction of the flow, as observed in the distribution of the principal strains whose maximum extensions, namely  $\varepsilon_1$ , are oriented in such a direction as is approximately close to that of the ice flow.

The dilatation  $\Delta$  shown in Fig. 11 is a two-dimensional one, that is the ratio of the change in area to the original area. Suppose that a circle with a unit radius was deformed into an ellipse. The area of the circle is equal to  $\pi$ ; the area of the ellipse is  $\pi(1+\varepsilon_1)(1+\varepsilon_2)$ , since the lengths of the axes of the ellipse are  $1+\varepsilon_1$  and  $1+\varepsilon_2$ . If the absolute values of  $\varepsilon_1$  and  $\varepsilon_2$  are both small, neglecting the small quantity of the products  $\varepsilon_1\varepsilon_2$ , the dilatation is given as follows:

$$\Delta = \pi(1+\varepsilon_1)(1+\varepsilon_2)/\pi - 1 = \varepsilon_1 + \varepsilon_2. \quad (9)$$

The positive value of the dilatation signifies that extension of strain is superior to contraction; the negative value signifies that contraction is superior to extension. The positive dilatation was observed in most parts of the triangulation chain, except in the regions of the surface depressions as shown in Figs. 7, 8, 9 and 10.

The maximum shear strain  $\gamma_{\max}$  of the surface of the ice sheet is approximately equal to  $\varepsilon_1 - \varepsilon_2$ , if the absolute values of  $\varepsilon_1$  and  $\varepsilon_2$  are both small. The value of  $\gamma_{\max}$  showed its peak at places where the horizontal velocity of ice flow varied considerably. From the distribution of  $\dot{\gamma}_{\max}$ , a boundary between different modes of ice movement was deduced to exist at around  $38^{\circ}10'E$ , while the surface divide of the drainages was determined at about  $37^{\circ}10'E$  (SHIMIZU *et al.*, 1978).

Rates of rotation  $\dot{\omega}$ , which were shown in Table 3, gave rather large values such as 0.02 degree/year in the region near  $36^{\circ}35'E$ ; 0.015 degree/year, that is about 1 min/year, in  $38^{\circ}20'E$ . These regions coincided well with those where the rates of the shear strain were very large. In the other places, rates of rotation were smaller than 30 s/year, which correspond to about  $1.5 \times 10^{-4}$  rad/year. Mean square error of the rate of rotation was estimated as 10 s/year in the maximum.

## 6. Vertical Flow and Mass Budget

The vertical flow velocity  $V_v$  which was obtained by eq. (7) is plotted in

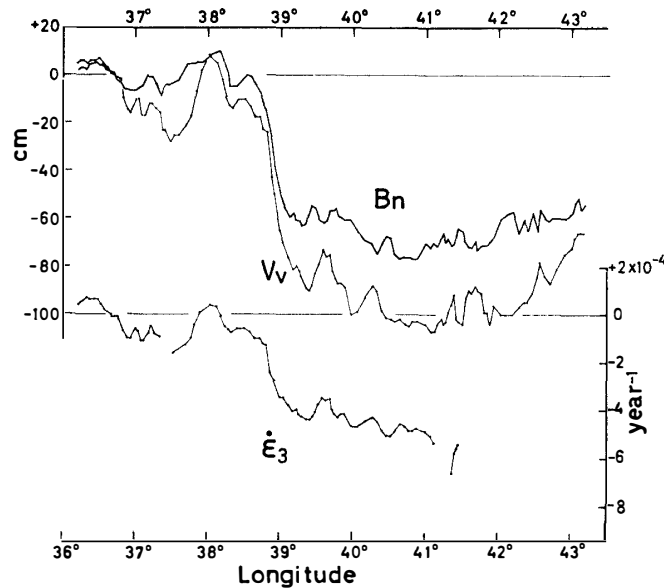


Fig. 12. Variations of the vertical velocity  $V_v$  in cm/year, the vertical strain rate  $\dot{\epsilon}_3$  in 1/year, and the net budget of ice  $B_n$  in  $\text{g}/\text{cm}^2 \cdot \text{year}$ .

Fig. 12 against the longitude along the chain from the east end of the Yamato Mountains to S240. The variation of  $V_v$  was slightly smoothed out by the application of the running mean over three stations. The following are the results shown distinctly by the figure:

(1) Positive velocities which signify upward motion of ice were noticed in the regions around  $36^\circ 30' \text{E}$  and  $38^\circ \text{E}$ . An annual net accumulation was negative in the former region, which represents ablation mainly due to sublimation of the exposed surface ice. It is consistent with the “emergence flow” often observed in the ablation area of a glacier. As for the latter region, a net accumulation was likewise smaller than other regions.

(2) In most parts except the above regions, negative velocities indicative of downward motion were observed and net accumulations were positive, showing that the “submergence flow” takes place in the accumulation area.

(3) The absolute value of  $V_v$  increased suddenly near  $39^\circ \text{E}$  where the horizontal component of velocity was close to the maximum value, and then it decreased gradually from  $42^\circ \text{E}$  eastward.

The average vertical strain rate  $\dot{\epsilon}_3$  of the ice sheet from the surface to the bedrock can be represented also by

$$\dot{\epsilon}_3 = V_v / I, \quad (10)$$

where  $I$  is the ice thickness measured by the radio echo sounder (SHIMIZU *et al.*, 1972; NARUSE and YOKOYAMA, 1975). Variation of  $\dot{\epsilon}_3$  is also shown in Fig. 12.

Now, consider the vertical column of ice with a unit cross area from the surface of the ice sheet to the bedrock. Downward motion of the surface of the ice sheet is considered to have resulted from densification of snow in the upper layer of the ice sheet and also from outflow of ice from the vertical column to the surroundings, while upward motion is considered to have resulted from inflow of ice into the column from the surroundings.

In order to obtain the mass budget at each triangulation station, the income of ice mass to the vertical column has to be compared with the outgo of ice mass from the column. Densification does not cause any change of mass of the column. Assuming that no melting of ice occurred at the bottom of the ice sheet, the net mass budget  $B_n$  per year is given as follows:

$$B_n = A_n \rho_s + (V_v - \dot{\delta}) \rho_i, \quad (11)$$

where  $A_n$  is the thickness of annual net accumulation of snow,  $\rho_s$  the density of deposited snow on the surface,  $\rho_i$  the density of ice in deep layers, and  $\dot{\delta}$  the rate of surface lowering due to densification of snow layers per year. One should take notice of the signs of the terms in eq. (11): the positive sign of  $B_n$  signifies the gain of mass and the negative the loss; the positive sign of  $V_v$  indicates upward flow and the negative downward; only the negative sign of  $\dot{\delta}$  is significant.

Rate of surface lowering due to densification of snow is unknown in the region of the triangulation chain. The vertical distribution of density was obtained from the surface down to 130 m at Mizuho Camp (NARITA and NAKAWO, unpublished). Density increased from 0.4 g/cm<sup>3</sup> at the surface to 0.83 g/cm<sup>3</sup> at 50 m below the surface. Using the equation of non-Newtonian densification of snow derived by BADER (1962), and assuming the appropriate value for the compactive viscosity factor with the variation of density (BADER, 1962; KOJIMA, 1964), the rate of densification of the upper 50 m layer of snow at Mizuho Camp was calculated to be about 10 to 20 cm per year. The average annual net accumulation there over a number of years was estimated to be about 10 g/year by a core analysis (NARITA and NAKAWO, unpublished). From the above results, the settling of the surface by densification was estimated to be roughly in the range from 0 to 30 cm/year, when the annual net accumulation is in the range from 0 to 20 g/year. The value of  $\rho_s$  was taken as 0.4 g/cm<sup>3</sup> as normally observed in the surface layer of snow in Mizuho Plateau, and  $\rho_i$  was 0.85 g/cm<sup>3</sup>. Substituting the respective value of  $\dot{\delta}$  for eq. (11), the net mass budget was calculated at each triangulation station.

Variation of the mass budget  $B_n$  is shown in Fig. 12. In the region from 39°E westward, the value of  $B_n$  was close to 0 cm/year; while in the region eastward, the value was strongly negative showing substantial mass deficits. It follows that the ice sheet along the triangulation chain from 39°E eastward was

not in the equilibrium state.

The above estimates of the mass budget might have large errors due to erroneous estimation of the densification rate. However, the observational results showed that the vertical velocity of surface flow was close to  $-100$  cm/year, namely 1 m/year of the submergence velocity, in the region from  $40^{\circ}\text{E}$  to  $42^{\circ}\text{E}$ , with the estimated error of 25%. The annual net accumulation averaged at the 44 triangulation stations in the region of  $40^{\circ}$ – $42^{\circ}\text{E}$  and over the 4-year period from 1969 to 1973–1974 was 20 cm/year in thickness of snow. Assuming the maximum probable error in the vertical velocity, namely 25 cm/year, the supply of snow on the surface of the ice sheet was still insufficient to maintain a stable condition of the ice sheet. It is certain that the ice sheet was shrinking along a part of the chain during this observation period. However, the surface lowering was not necessarily taking place over the entire area of Mizuho Plateau. It is possible that the thinning of the ice was rather local occurrence. In this regard, the propagation of a kinematic wave (LIGHTHILL *et al.*, 1955) can be imagined, which was propagating the perturbation of the ice condition.

FEDERER *et al.* (1970) obtained also the result of mass deficit in the amount of 10 cm/year during ten years from 1959 to 1968, in the inclined shaft of 40 m deep at Jarl-Joset Station, Greenland ice sheet. After NYE (1975) proposed a better model to calculate the surface lowering of the ice, FEDERER and SURY (1976) corrected the value of mass deficit as 7.7 cm/year. While it was estimated that the ice sheet is currently thinning by about 0.4 m/year at Byrd Station, Antarctica (HUGHES, 1973; WHILLANS, 1973), and the ice shelf is growing thicker by almost 1 m/year in the vicinity of the grounding line of the Ross Ice Shelf (THOMAS, 1976).

The results of the above studies clearly indicate that the ice sheet is never in a steady condition in response to a recent variation of climate, that is mainly of precipitation.

### **7. Relation between Surface Flow and Topography**

Measurements of surface slopes of the ice sheet were carried out at each triangulation station: the vertical angle of the skyline was measured by a theodolite in ten directions from a station. The distance from a station to the skyline varied considerably in different directions due to the middle or small scale surface undulation of the ice sheet. Consequently, the vertical angle of the skyline does not indicate the surface slope in a unique way. However, the pattern of the radial distribution of the vertical angle of the skyline from a station shows the surface feature of the ice sheet surrounding the station. The surface features could be divided into characteristic four types by using the data of the skyline measurements, as follows:

(1) Sheet with even slope: Stations A023, A031, A035, A039, A043, A045, A047, A049, A051, A054, A057, A059, A062, A063, A064, A066, A067, A069, A070, A071, A073, A077, A080, A082, A084, A089, A092, A097, A100, A101, A102, A105, A108, A110, A112, A120, A125, A126, A130, A144, A148, and A154.

(2) Ridge or mound: Stations A032, A036, A040, A044, A048, A052, A056, A060, A068, A072, A079, A083, A095, A111, A118, A127, A131, A147, A155 and A159.

(3) Trough or depression: Stations A065, A093, A124, A134, A136, A138, A141, A143, A153, A156, A158 and A160.

(4) Irregular undulation: Stations A003–A022, A030, A061 and A094.

While, at the other stations than the above, the surface relief indicated an intermediate type between the above three features or irregular undulation. The typical examples of these types of the surface relief are shown in Fig. 13 by the data of A062, A036, A138 and A022, respectively.

The surface dilatation was obtained as positive value, that is tensile strain, on

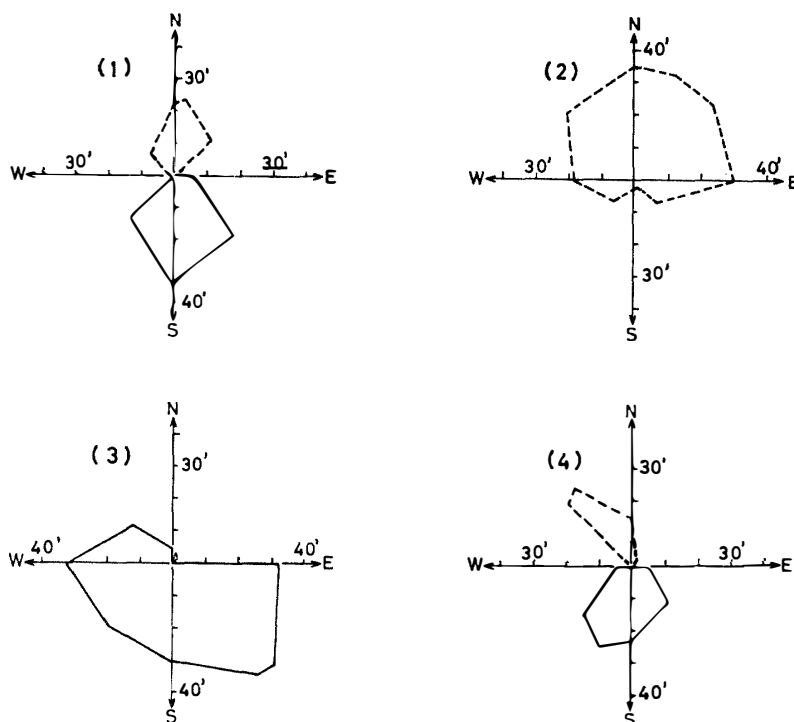


Fig. 13. Distribution of surface slopes (unit: minute) in 8~10 directions from a station obtained by the skyline measurement. Dotted line shows negative slope; solid line positive slope. (1) Sheet with even slope at A062, (2) ridge or mound at A036, (3) trough or depression at A138, and (4) irregular undulation at A022.

the ridge or mound; negative value, that is compressive strain, in the trough or depression of the surface. While the maximum shear strain showed large value on the surface with remarkable undulations.

Relation between the direction of the maximum surface slope and that of surface flow was examined as for the 42 points on the ice sheet with even slope, as shown in Fig. 14. The direction of the surface slope was obtained by averaging the direction of the maximum uphill slope and that of downhill slope from

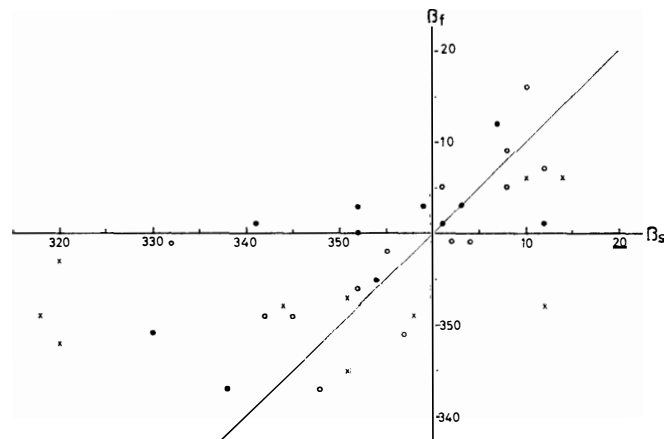


Fig. 14. Relation between direction of surface flow  $\beta_f$  (degree) and that of maximum surface slope  $\beta_s$  (degree).

Both directions are represented clockwise from north.

Solid circles indicate the values on the slope of more than  $1/150$  ( $\approx 23$  min); white circles on that of more than  $1/200$  ( $\approx 17$  min); cross marks on that of less than  $1/200$ . The values were obtained at the 42 triangulation stations on the ice sheet with even slopes.

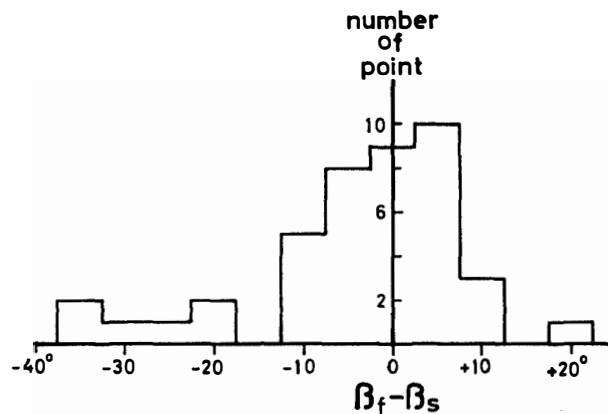


Fig. 15. Histogram of the differences between direction of surface flow of ice  $\beta_f$  (degree) and that of maximum surface slope  $\beta_s$  (degree) on the ice sheet with even slope.

the data of the skyline measurements. It is noticed in Fig. 14 that the correlation between the direction of the ice flow and that of surface slope is better where the surface slope is larger than 1/200 (17 min). Fig. 15 shows the frequency distribution of the difference between flow and slope directions. Standard deviation of the direction of the ice flow from the direction of surface slope was 12.4 degrees for 42 points with even slope; and 8.9 degrees for 30 points of even slope of more than 1/200. Close coincidence of flow and slope directions did not hold for mound terrain, depression terrain or irregular undulating terrain.

If it is assumed that the ice sheet does not slide on the bed; namely, ice movement consists only of deformation within the ice sheet due to its weight, the following simple relation between surface velocity  $V_h$ , ice thickness  $I$  and surface slope  $\theta_s$  is derived (NYE, 1952):

$$V_h = \frac{2A}{n+1} (\rho g \sin \theta_s)^n I^{n+1}, \tag{12}$$

where  $g$  is the gravitational acceleration,  $\rho$  the density of ice, and  $A$  and  $n$  are the parameters in flow-law of ice (GLEN, 1955). Substituting the adequate value

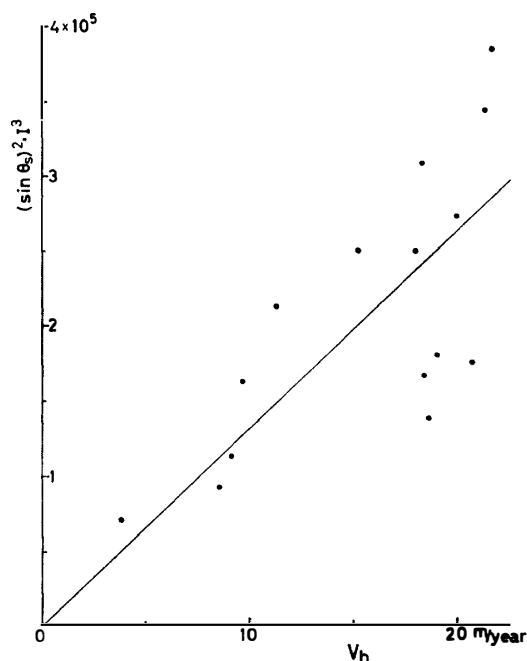


Fig. 16. Relation between measured values of horizontal velocity  $V_h$  (m/year) and calculated values of  $(\sin \theta_s)^2 \cdot I^3$  on the ice sheet with even slope.

$\theta_s$ : Mean value of the uphill and downhill slope of the ice sheet surface (degree).

$I$ : Ice thickness (m).

of  $n$  from 1 to 4 as usually estimated for glacier ice into eq. (12), the relation was examined between the measured value of  $V_h$  and the value of  $(\sin \theta_s)^n \cdot I^{n+1}$  at the 15 stations on the ice sheet with even slope described above. The value of  $\theta_s$  was the mean of uphill slope and downhill slope obtained by the skyline measurements; the ice thickness was from the radio echo sounding. Correlation coefficient between  $V_h$  and  $(\sin \theta_s)^n \cdot I^{n+1}$  was somewhat larger in the case that  $n$  was equal to the value from 2 to 3. Fig. 16 shows the relation between  $V_h$  and  $(\sin \theta_s)^2 \cdot I^3$ . Correlation coefficient between these values was 0.72; the standard deviation of the calculated value  $(\sin \theta_s)^2 \cdot I^3$  from a regression line was  $0.67 \times 10^5 \text{ m}^3$ ; the relative standard deviation, namely the deviation divided by the mean value of  $(\sin \theta_s)^2 \cdot I^3$ , was 0.32. A large scattering in the relation of Fig. 16 is recognized; it is considered to have resulted from the errors included in the value of surface slope, in ice thickness and also in the assumption of eq. (12). Very little correlation was observed between  $V_h$  and  $(\sin \theta_s)^n \cdot I^{n+1}$ , when eq. (12) was applied to stations on the ice surface with mound, depression, or irregular undulation.

It can be concluded, however, that the relation, namely  $V_h \propto (\sin \theta_s)^2 \cdot I^3$ , becomes useful to predict the approximate velocity from the values of ice thickness and surface slope on the even ice sheet, wherever the direct measurements of the surface flow were not available.

### 8. Concluding Remarks

Described in this paper are firstly the method of the triangulation survey in Section 2, that of data reductions in Section 3, and that of calculations of flow and strain in Section 4. The methods were based on standard techniques for topographic mapping or measurement of the earth surface strain. Therefore, the author is convinced that the results with relatively high accuracies were obtained from the survey even though the triangulation chain extended 250 km from a fixed reference of ice-free rock.

Results on the three components of the surface flow vectors at 141 points and also on various parameters as to surface strains at 140 triangles are secondly shown in detail in Sections 5, 6 and 7, with some discussions on distribution of flow vectors and strains; mass budget of ice; and the relation between the surface feature of the ice sheet and flow velocity. Estimation of the ice mass flux which passes across the chain towards the coast and flow lines over Mizuho Plateau are given in another article (NARUSE and SHIMIZU, 1978).

### Acknowledgements

The author would like to express his appreciation to Dr. T. ISHIDA, Dr.

A. HIGASHI and Dr. H. SHIMIZU of Hokkaido University, and Dr. C. F. RAYMOND of University of Washington for their helpful advice and comments on this paper.

#### References

- BADER, H. (1962): Theory of densification of dry snow on high polar glaciers, 2. CRREL Res. Rep., **108**, 18 p.
- FEDERER, B., SURY, H., PHILBERTH, K. and QUERVAIN, M. de (1970): Outflow and accumulation of ice in Jarl-Joset Station, Greenland. *J. Geophys. Res.*, **75**(24), 4567–4569.
- FEDERER, B. and SURY, H. (1976): Deducing thickness changes of an ice sheet: comments on the paper by J. F. NYE. *J. Glaciol.*, **17**(77), 531.
- GLEN, J. W. (1955): The creep of polycrystalline ice. *Proc. R. Soc. London*, **A228**, 519–538.
- HARADA, T. (1966): Universal program to be used with electronic computer for net-adjustment of any geodetic figure. *Bull. Geogr. Surv. Inst.*, **12**(1), 21–39.
- HUGHES, T. (1973): Is the west antarctic ice sheet disintegrating?. *J. Geophys. Res.*, **78**(33), 7884–7910.
- JAEGER, J. C. (1969): *Elasticity, Fracture and Flow: with Engineering and Geological Applications*, 3rd ed. London, Methuen, 268 p.
- KOJIMA, K. (1964): Densification of snow in Antarctica. *Antarctic Snow and Ice Studies*, Washington, D.C., Am. Geophys. Union, 157–218 (*Antarct. Res. Ser.*, **2**).
- LIGHTHILL, M. J. and WHITHAM, G. B. (1955): On kinematic waves. II. A theory of traffic flow on long crowded roads. *Proc. R. Soc. London*, **A229**, 317–345.
- NARUSE, R., YOSHIMURA, A. and SHIMIZU, H. (1972): Installation of a triangulation chain and a traverse survey line on the ice sheet in the Mizuho Plateau—West Enderby Land area, East Antarctica, 1969–1970. *JARE Data Rep.*, **17** (*Glaciol.*), 111–131.
- NARUSE, R. (1975): Movement of the ice sheet observed by a triangulation chain. *JARE Data Rep.*, **28** (*Glaciol.*), 48–61.
- NARUSE, R. and YOKOYAMA, K. (1975): Position, elevation and ice thickness of stations. *JARE Data Rep.*, **28** (*Glaciol.*), 7–47.
- NARUSE, R. and SHIMIZU, H. (1978): Flow line of the ice sheet over Mizuho Plateau. *Mem. Natl Inst. Polar Res., Spec. Issue*, **7**, 227–234.
- NYE, J. F. (1952): The mechanics of glacier flow. *J. Glaciol.*, **2**(12), 82–93.
- NYE, J. F. (1975): Deducing thickness changes of an ice sheet from radio-echo and other measurements. *J. Glaciol.*, **14**(70), 49–56.
- SATOW, K. (1977): Resurvey of strain grids at Mizuho Camp and Y200. *JARE Data Rep.*, **36** (*Glaciol.*), 139–141.
- SHIMIZU, H., NARUSE, R., OMOTO, K. and YOSHIMURA, A. (1972): Position of stations, surface elevation and thickness of the ice sheet, and snow temperature at 10 m depth in the Mizuho Plateau-West Enderby Land area, East Antarctica, 1969–1971. *JARE Data Rep.*, **17** (*Glaciol.*), 12–37.
- SHIMIZU, H., YOSHIMURA, A., NARUSE, R. and YOKOYAMA, K. (1978): Morphological feature of the ice sheet in Mizuho Plateau. *Mem. Natl Inst. Polar Res., Spec. Issue*, **7**, 14–25.
- SHIRAISHI, K., NARUSE, R. and KUSUNOKI, K. (1976): Collection of Yamato meteorites, Antarctica, in December 1973. *Nankyoku Shiryo (Antarct. Rec.)*, **55**, 49–60.
- THOMAS, R. H. (1976): Thickening of the Rose Ice Shelf and equilibrium state of the West Antarctic ice sheet. *Nature*, **259**, 180–183.
- WHILLANS, I. M. (1973): State of equilibrium of the West Antarctic inland ice sheet. *Science*, **182**, 476–479.
- YANAI, K. (1976): 1974-nen no nankyoku-san Yamato in-seki no tansa to saishû (Search and

- collection of Yamato meteorites, Antarctica, in October and November 1974). Nankyoku Shiryo (Antarct. Rec.), **56**, 70-81.
- YOKOYAMA, K. (1975): Net accumulation by stake measurements. JARE Data Rep., **28** (Glaciol.), 62-82.
- YOSHIDA, M., ANDO, H., OMOTO, K., NARUSE, R. and AGETA, Y. (1971): Discovery of meteorites near Yamato Mountains, East Antarctica. Nankyoku Shiryo (Antarct. Rec.), **39**, 62-65.

*(Received June 7, 1977)*